

Argon Laser Retinal Lesions Evaluated In Vivo by Optical Coherence Tomography

CYNTHIA A. TOTH, MD, REGINALD BIRNGRUBER, PhD,
STEPHEN A. BOPPART, MSEE, MICHAEL R. HEE, MSEE,
JAMES G. FUJIMOTO, PhD, CHERYL D. DICARLO, DVM,
ERIC A. SWANSON, PhD, CLARENCE P. CAIN, PhD,
DREW G. NARAYAN, GARY D. NOOJIN,
AND WILLIAM P. ROACH, PhD

- **PURPOSE:** To assess the in vivo evolution of argon laser retinal lesions by correlating the cross-sectional structure from sequential optical coherence tomography with histopathologic sectioning.
- **METHODS:** Argon laser lesions were created in the retinas of *Macaca mulatta* and evaluated by cross-section optical coherence tomography, which was compared at selected time points with corresponding histopathology.
- **RESULTS:** Argon laser lesions induced an optical coherence tomography pattern of early outer retinal relative high reflectivity with subsequent surrounding relative low reflectivity that correlated well with histopathologic findings. The in vivo

optical coherence tomography images of macular laser lesions clearly demonstrated differences in pathologic response by retinal layer over time.

- **CONCLUSION:** The novel sequential imaging of rapidly evolving macular lesions with optical coherence tomography provides new insight into the patterns of acute tissue response by cross-sectional layer. This sequential imaging technique will aid in our understanding of the rapid evolution of retinal pathology and response to treatment in the research and clinical setting.

WE ARE INTERESTED IN UNDERSTANDING THE initial laser tissue interaction created by timed argon laser exposure directed to the retina. Previous studies analyzed laser lesions by direct observation and photographs of the retina, histopathologic assessment of retinal effects, and attempts to assess function, such as fluorescein leakage at the laser site, chorioretinal adhesion, and cellular activity after laser treatment.^{1,4} The effects of argon, ruby, krypton, and dye laser energy on different layers of the retina and choroid have been shown in histopathologic studies of lesions typically 1 hour to 24 hours old in rabbits, primates, and human beings.¹⁻¹⁰ Because of a time delay of minutes to hours, these studies viewed a combination of the direct effects of the laser energy along with secondary physiologic responses after laser delivery. That response, such as edema and inflammation, may mask or amplify the initial laser effect. In addition, processing tissue for histopathologic evaluation may add artifacts to the lesions.

Accepted for publication Sept 24, 1996.

From the Department of Ophthalmology, Duke University School of Medicine, Durham, North Carolina (Dr Toth and Mr Narayan); Medizinisches Laserzentrum Lübeck, Lübeck, Germany (Dr Birngruber); Department of Electrical Engineering, Research Laboratory of Electronics, Massachusetts Institute of Technology, Cambridge, Massachusetts (Mr Boppart, Mr Hee, and Dr Fujimoto), and Lincoln Laboratory (Dr Swanson); Uniformed Services University of the Health Sciences, Bethesda, Maryland (Dr DiCarlo); The Analytical Sciences Corporation, San Antonio, Texas (Dr Cain and Mr Noojin); and Air Force Office of Scientific Research, Chemistry and Life Science, Bolling AFB, District of Columbia (Dr Roach). This research was sponsored by USAF Armstrong Laboratory, the Air Force Office of Scientific Research, Air Force Systems Command, USAF, under grant numbers F49620-95-1-0226 and 2312AA-92AL014 and contract F33615-92-C-0017. The US Government is authorized to reproduce and distribute reprints for governmental purposes notwithstanding any copyright notation thereon. The views and conclusions contained in this document are those of the authors and should not be interpreted as necessarily representing the official policies or endorsements, either express or implied, of the Air Force Office of Scientific Research (AFOSR) or the US Government.

Reprint requests to Cynthia A. Toth, MD, Duke University Eye Center, Box 3802, Durham, NC 27710; fax: (919) 681-6474; e-mail: toth0004@mc.duke.edu

Lorenz⁵ addressed the issue of identifying the earliest time point of tissue response to argon laser application. Lorenz studied the rabbit retinal morphologic characteristics with immediate perfusion fixation of tissue after laser lesion placement. This provided a 20-second fixed lesion but not serial analysis of individual lesion development. To accomplish this, we used noninvasive optical coherence tomography, which utilizes backscattering or reflections of light analogous to the way ophthalmic ultrasound uses sound reflections to create an image. We evaluated optical coherence tomography images acquired from argon laser retinal lesions as they evolved over seconds, minutes, and days after laser delivery, compared these with light microscopic appearance, and found new information about the initial evolution of retinal laser lesions.

METHODS

Macaca mulatta weighing from 3 to 4 kg were maintained at a laboratory animal facility fully accredited by the American Association for the Accreditation of Laboratory Animal Care. The animals were used in accordance with federal regulations, the *Care and Use of Animals* (National Institutes of Health publication no. 86-23), and the Association for Research in Vision and Ophthalmology Resolution on the Use of Animals in Ophthalmic and Vision Research.

Each animal was given a preanesthetic dose of 10 mg/kg of intramuscular ketamine hydrochloride and 0.25 mg/kg of subcutaneous atropine sulfate. Proparacaine hydrochloride 0.5%, phenylephrine hydrochloride 2.5%, and tropicamide 1% were administered to the treatment eye. Anesthesia was induced with an initial dose of propofol (up to 5 mg/kg) administered to effect and maintained with 0.15 to 0.5 mg/kg/hour of propofol via syringe pump. Heart rate, blood pressure, temperature, and pulse were continuously monitored. The airway was maintained with an endotracheal tube. Peribulbar injection of 0.5 ml of a 50-50 mixture of lidocaine 2% and bupivacaine 0.75% with hyaluronidase was administered to the treatment eye to reduce extraocular muscular movement. The cornea was irrigated with sterile saline solution as needed to prevent desiccation. At selected time points, immediately before euthanasia and while

the animal was under deep anesthesia, the laser-treated eye was enucleated. The animals were euthanized while under deep propofol anesthesia, with an overdose of pentobarbital administered intravenously. The globe was incised anterior to the equator and immersed in 3% glutaraldehyde with 0.1 M sodium cacodylate buffer. Within 10 minutes, the posterior eye cup was dissected while immersed.

Five eyes of three animals were used for the in vivo and histologic study of 17 argon laser lesions. The second eye of two animals received argon laser lesions while under anesthesia, followed by euthanasia. All 17 argon laser lesions were fixed for histopathologic evaluation. At the time of enucleation and fixation, 10 lesions were 1 hour old, two lesions were 1 day old, two lesions were 2 days old, and three lesions were 8 days old. Because laser lesions are known to change significantly during the first hour,⁵ lesions 1 day old and older were used for the initial morphologic comparison. The morphologic characteristics of the older lesions would not be expected to change during the hour between optical coherence tomography imaging of the lesion and fixation.

Except as noted in the Table, lesions were created with 330 to 500 mW of argon blue-green laser for 100 or 200 msec delivered to the cornea, with an estimated retinal spot size of 50 μ m. Before delivery, the argon aiming beam and the optical coherence tomography beam were colinearly aligned to ensure that the horizontal optical coherence tomography scan would fall over the center of the newly formed lesion. After laser delivery, the location of the optical coherence tomography scanning beam was monitored by a videotape camera configured to the slit lamp. Optical coherence tomography images were temporally acquired in 5-second intervals during the first minute, at 1- to 5-minute intervals during the first hour, and then in selected eyes at days 1, 2, and 8 after argon laser delivery.

Optical coherence tomography permits high resolution, cross-sectional, tomographic imaging of biologic microstructure by directing a focused beam of light into the biologic tissue and measuring the delay time (echo delay) for the backscattered light to return to the instrument. Light that is backscattered or reflected from structural features at varying depths within the specimen is measured to yield longitudinal (depth) information on tissue structures. A cross-

Table. Argon Laser Retinal Lesions Evaluated by Optical Coherence Tomography

Lesion	Argon Laser Beam Variables			Interval Between Laser Lesion and Enucleation
	Energy (mW)	Duration (msec)	Retinal Spot Size (μm)	
1	110	200	65	1 hr
2	160	200	125	1 hr
3	330	100	50	1 hr
4	330	200	50	1 hr
5	330	200	50	1 hr
6	330	200	50	1 hr
7	380	100	50	1 hr
8	380	100	50	1 hr
9	380	100	50	1 hr
10	500	200	50	1 hr
11	380	100	50	1 day
12	380	100	50	1 day
13	200	200	50	2 days
14	500	100	50	2 days
15	356	100	50	8 days
16	380	100	50	8 days
17	380	100	50	8 days

sectional image of the specimen is constructed in a manner similar to radar imaging by laterally scanning the light beam through the specimen and displaying longitudinal (depth) information from different adjacent transverse positions. Because the velocity of light is extremely high, the echo delay time cannot be measured directly by electronics; an optical technique known as low-coherence interferometry is used. The measurement system consists of a low-coherent, superluminescent diode 840-nm light source in conjunction with a fiber optic Michelson interferometer. The optical detection method used in optical coherence tomography yields very high sensitivity. The system achieves a signal-to-noise ratio of 109 dB, defined by measuring the maximum signal when the optical beam is reflected from a highly reflective mirror and dividing by the instrument noise level. This signal-to-noise ratio also determines the dynamic range that can be imaged. The fact that optical coherence tomography uses low-coherence light and detects light at selected echo time delays greatly discriminates against the detection of light that is multiply scattered.

Optical coherence tomography-generated images are representations of tissue structure based on the optical backscattered intensity, which is highly de-

pendent on the optical properties of the structure. Optical coherence tomography images have artifacts that arise from optical attenuation with depth, shadowing, and refractive index effects. However, when measurements are performed in a consistent manner, these effects are considered part of the baseline. The diagnostic power of the imaging technique relies on detecting deviations from this baseline.

Lesions were identified, dissected from the fixed posterior eye cups with a surrounding zone of non-treated tissue, and marked so that the orientation of the lesion could be determined during sectioning. Tissue was embedded in Spurr's resin, sectioned at a 1- μm thickness, and stained with methylene blue for light microscopy. Light micrographs of a horizontal central section of each lesion were captured digitally for analysis. The sections were photographed with 35-mm black-and-white film for publication.

Using Adobe Photoshop 3.0, the central horizontal light micrograph was matched to the corresponding in vivo optical coherence tomographic image for each lesion. A 250- μm measurement was recorded horizontally and vertically on each light micrograph and vertically on each optical coherence tomography image. The light micrograph was then matched to the optical coherence tomography image magnification.

Lorenz⁵ addressed the issue of identifying the earliest time point of tissue response to argon laser application. Lorenz studied the rabbit retinal morphologic characteristics with immediate perfusion fixation of tissue after laser lesion placement. This provided a 20-second fixed lesion but not serial analysis of individual lesion development. To accomplish this, we used noninvasive optical coherence tomography, which utilizes backscattering or reflections of light analogous to the way ophthalmic ultrasound uses sound reflections to create an image. We evaluated optical coherence tomography images acquired from argon laser retinal lesions as they evolved over seconds, minutes, and days after laser delivery, compared these with light microscopic appearance, and found new information about the initial evolution of retinal laser lesions.

METHODS

Macaca mulatta weighing from 3 to 4 kg were maintained at a laboratory animal facility fully accredited by the American Association for the Accreditation of Laboratory Animal Care. The animals were used in accordance with federal regulations, the *Care and Use of Animals* (National Institutes of Health publication no. 86-23), and the Association for Research in Vision and Ophthalmology Resolution on the Use of Animals in Ophthalmic and Vision Research.

Each animal was given a preanesthetic dose of 10 mg/kg of intramuscular ketamine hydrochloride and 0.25 mg/kg of subcutaneous atropine sulfate. Proparacaine hydrochloride 0.5%, phenylephrine hydrochloride 2.5%, and tropicamide 1% were administered to the treatment eye. Anesthesia was induced with an initial dose of propofol (up to 5 mg/kg) administered to effect and maintained with 0.15 to 0.5 mg/kg/hour of propofol via syringe pump. Heart rate, blood pressure, temperature, and pulse were continuously monitored. The airway was maintained with an endotracheal tube. Peribulbar injection of 0.5 ml of a 50-50 mixture of lidocaine 2% and bupivacaine 0.75% with hyaluronidase was administered to the treatment eye to reduce extraocular muscular movement. The cornea was irrigated with sterile saline solution as needed to prevent desiccation. At selected time points, immediately before euthanasia and while

the animal was under deep anesthesia, the laser-treated eye was enucleated. The animals were euthanized while under deep propofol anesthesia, with an overdose of pentobarbital administered intravenously. The globe was incised anterior to the equator and immersed in 3% glutaraldehyde with 0.1 M sodium cacodylate buffer. Within 10 minutes, the posterior eye cup was dissected while immersed.

Five eyes of three animals were used for the in vivo and histologic study of 17 argon laser lesions. The second eye of two animals received argon laser lesions while under anesthesia, followed by euthanasia. All 17 argon laser lesions were fixed for histopathologic evaluation. At the time of enucleation and fixation, 10 lesions were 1 hour old, two lesions were 1 day old, two lesions were 2 days old, and three lesions were 8 days old. Because laser lesions are known to change significantly during the first hour,⁵ lesions 1 day old and older were used for the initial morphologic comparison. The morphologic characteristics of the older lesions would not be expected to change during the hour between optical coherence tomography imaging of the lesion and fixation.

Except as noted in the Table, lesions were created with 330 to 500 mW of argon blue-green laser for 100 or 200 msec delivered to the cornea, with an estimated retinal spot size of 50 μm . Before delivery, the argon aiming beam and the optical coherence tomography beam were colinearly aligned to ensure that the horizontal optical coherence tomography scan would fall over the center of the newly formed lesion. After laser delivery, the location of the optical coherence tomography scanning beam was monitored by a videotape camera configured to the slit lamp. Optical coherence tomography images were temporally acquired in 5-second intervals during the first minute, at 1- to 5-minute intervals during the first hour, and then in selected eyes at days 1, 2, and 8 after argon laser delivery.

Optical coherence tomography permits high resolution, cross-sectional, tomographic imaging of biologic microstructure by directing a focused beam of light into the biologic tissue and measuring the delay time (echo delay) for the backscattered light to return to the instrument. Light that is backscattered or reflected from structural features at varying depths within the specimen is measured to yield longitudinal (depth) information on tissue structures. A cross-

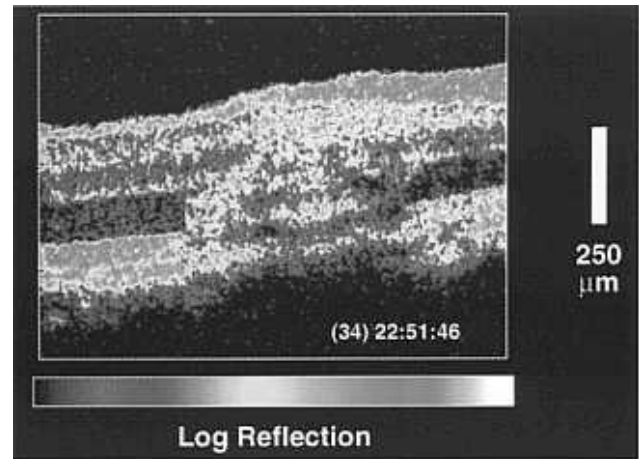


Figure 1. (Left) Light micrographs of 1-day-old 380-mW argon laser retinal lesion with full-thickness retinal damage and splitting of the internal limiting membrane and the disrupted nerve fiber layer. Nasal retina is to the right side of the image, where the nerve fiber layer is thicker. The retinal surface is domed over the lesion, with a necrotic central cleft in each lesion associated with an artifact of focal fixation separation. Inner and outer nuclear layers demonstrate a curving plane of displaced pyknotic nuclei domed over the central focus of more normal-appearing photoreceptors. At the margins of the lesion are increased intracellular vacuoles and extracellular spaces. The underlying retinal pigment epithelium demonstrates extensive intraretinal vacuoles and extracellular spaces. There is pigment displacement centrally over the area of abnormal retinal pigment epithelium. (Right) Optical coherence tomography of the 1-day lesion at a site corresponding to the section at left. The inner retinal layer of increased relative higher reflectivity is thicker at the nasal (right) side of the image and thins as the nerve fiber layer thins temporally. There is minimal sloping elevation of the anterior retinal surface over the center of the lesion. It does not demonstrate any inner limiting membrane or nerve fiber layer separation. There is a prominent focal loss of the normal retinal optical coherence tomography pattern in the plexiform and nuclear layers centrally. The lesion demonstrates a focal site of higher reflectivity corresponding to the necrotic photoreceptor site at the base of the lesion. This is surrounded by a zone of low reflectivity at the lateral margins that corresponds to the area of increased vacuole formation and extracellular fluid. At the temporal side of the lesion, there is a highly reflective area at the margin of the zone of low reflectivity at the level of the photoreceptors. This appears to correspond to the area of additional dense necrosis beyond the site of vacuolization.

RESULTS

THE OPTICAL COHERENCE TOMOGRAPHY OF THE NORMAL primate retina at the margins of these lesions appeared similar to that reported earlier.¹¹ Focal layers of relative high reflectivity corresponded to the location of the nerve fiber layer at the innermost position in the retina and to the choroid and retinal pigment epithelium together at the outer extent of the section. Additional layers of relative high reflectivity corresponded to the location of the plexiform layers, and layers of low reflectivity corresponded to nuclear and photoreceptor layers.

The light micrographs of the laser lesions demonstrated the classic appearance of argon laser retinal effects, with damage ranging from moderate to severe, full-thickness retinal damage.

At 1 day, light micrographs (Figure 1, left) of the lesions demonstrated full-thickness retinal damage, with splitting of the internal limiting membrane and the disrupted nerve fiber layer. The retinal surface was domed over the lesions, with a necrotic central cleft in each lesion associated with an artifact of focal fixation separation. Inner and outer nuclear layers demonstrated a curving plane of displaced pyknotic nuclei over the central focus of more normal-appearing photoreceptors. At the margins of the lesion were increased intracellular vacuoles and extracellular spaces. The underlying retinal pigment epithelium demonstrated extensive intraretinal vacuoles and extracellular spaces. Pigment was displaced centrally over the damaged retinal pigment epithelium.

At 1 day, optical coherence tomography (Figure 1, right) also demonstrated similar mild sloping eleva-

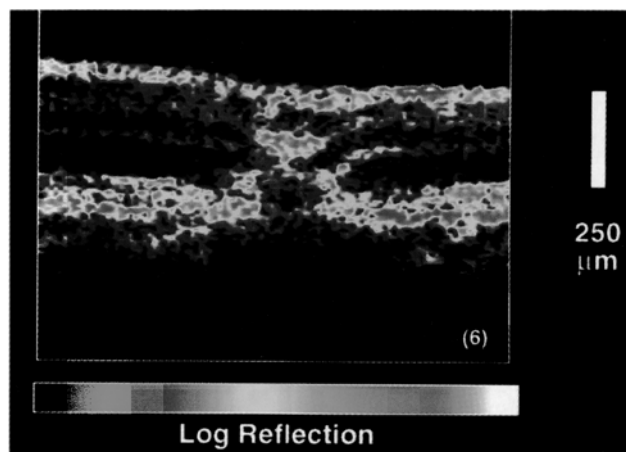
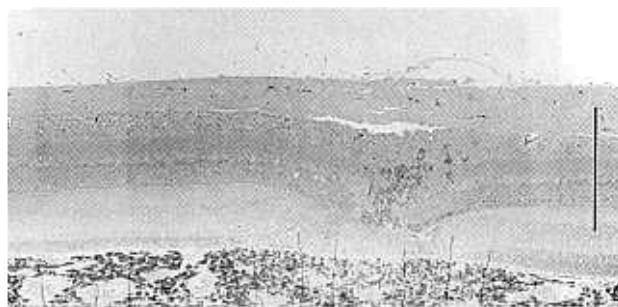


Figure 3. (Left) Light micrographs of 8-day-old 380-mW argon laser retinal lesion demonstrates pigment-containing macrophages and retinal pigment epithelium cells centrally within the lesion, with an outward bowing of the inner nuclear layer as the chorioretinal scar develops. Nasal retina is to the right side of the image. (Right) Optical coherence tomography of the 8-day lesion at a site corresponding to the section at left demonstrates high reflectivity, most prominent centrally in the outer plexiform layer with a "V" configuration of the outer nuclear layer corresponding to the distortion seen on histopathology. Where the photoreceptor outer segments have been replaced by fibrotic tissue, there is a margin of high reflectivity with a central focus of low reflectivity. Nasal retina is to the right side of the image.

of retinal pigment epithelium and photoreceptors, pyknotic photoreceptor nuclei, milder inner retinal damage with focal vacuoles and clefting in the nerve fiber layer, and no gross distortion of retinal layers. The optical coherence tomography of the 200-mW lesion at day 2 demonstrated focal high reflectivity over the photoreceptor layer similar to that in Figure 2, bottom. The nerve fiber layer and inner plexiform layer also had a smaller band of high reflectivity but without any separation of inner retinal layers. There was a zone of low reflectivity in the retinal pigment epithelium/choroidal layer directly beneath the laser lesion.

At 8 days, the light micrographs demonstrated pigment-containing macrophages and retinal pigment epithelium cells centrally within the three lesions (Figure 3, left). Fibrotic tissue replaced the central focus of necrotic photoreceptors, with an outward bowing of the inner nuclear layer in two lesions (Figure 3, left), which corresponded to a prominent "V" configuration centrally in the lesion as viewed by optical coherence tomography cross-section (Figure 3, right). Where the photoreceptor outer segments were replaced by fibrotic tissue, there was a margin of high reflectivity with a central focus of low reflectivity (Figure 3, right). In one lesion, the

light micrograph demonstrated photoreceptors separated from the retinal pigment epithelium by a serous elevation. In this lesion, the optical coherence tomography demonstrated a larger central site of low reflectivity rimmed by high reflectivity, with no outward bowing of the outer nuclear layer. At 8 days, optical coherence tomography demonstrated no retinal elevation at the laser site.

The histopathology at 1 hour (Figure 4, left) was compared with the optical coherence tomography of the same lesion performed at 1 minute 12 seconds after laser delivery (Figure 4, right). Thus there may have been significant lesion evolution between the recording of the optical coherence tomography and the fixation of the tissue. One-hour light micrographs of 380-mW, 100-msec argon lesions demonstrated full-thickness retinal damage in all lesions. In one lesion, there was massive displacement of outer retinal layers and central clefting at the level of the outer nuclear and outer plexiform layers, with minimal marginal vacuolization (Figure 4, left), compared with 1- and 2-day-old lesions (Figures 1, left, and 2, top). The optical coherence tomography (Figure 4, right) of this lesion, taken at 1 minute 12 seconds after argon laser delivery of the lesion seen in Figure 4, left, demonstrated outer retinal high reflectivity extending

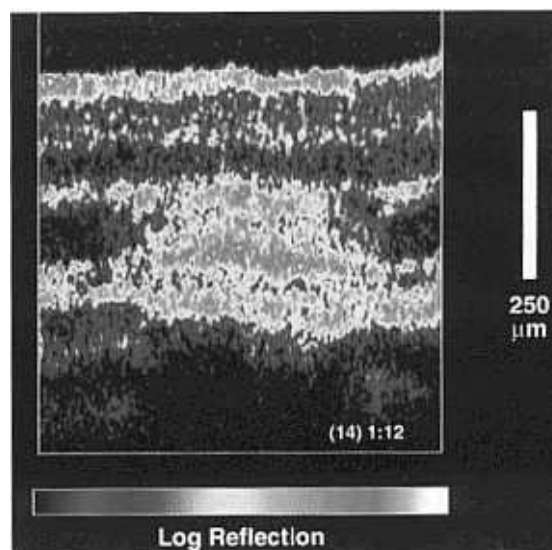


Figure 4. (Left) Light micrographs of 1-hour-old, 380-mW, 100-msec argon laser retinal lesion demonstrates massive displacement of outer retinal layers and central clefting at the level of the outer nuclear layer and outer plexiform layer. There is full-thickness retinal damage with minimal marginal vacuolization. Nasal retina is to the left side of the image. (Right) Optical coherence tomography of the 1-hour lesion performed at 72 seconds after laser delivery, at a site corresponding to the section at left, demonstrates outer retinal high reflectivity extending through the outer plexiform layer but no significant inner retinal changes, no low reflectivity in the retinal pigment epithelium/choroid, and no retinal elevation. Nasal retina is to the left side of the image.

through the outer plexiform layer but no significant inner retinal changes, no low reflectivity in the retinal pigment epithelium/choroid, and no retinal elevation (Figure 4, right). The other 1-hour lesions, when examined by optical coherence tomography during the first 1 to 4 minutes after argon laser delivery, showed a similar pattern of optical coherence tomography relative backscatter. The histopathology of the other 1-hour lesions demonstrated full-thickness damage and thickening of the retina over the center of the lesion but not the massive displacement of outer retinal layers and central clefting seen in Figure 4, left.

Another lesion fixed at 1 hour was a 500-mW, 200-msec argon lesion that developed a subretinal and vitreous hemorrhage within seconds after laser delivery. In the light micrographs, the retina is distorted by a large subretinal and intraretinal hemorrhage and has an overlying vitreous hemorrhage greater than 150- μ m in thickness (Figure 5, top). The optical coherence tomography of this lesion from 6 seconds through 15 minutes showed a bulging area

of intense high reflectivity that increased in size and corresponded to the preretinal blood. There was an intensely low reflectivity "shadow" behind this high-reflectivity site, with no images of the typical optical coherence tomography retinal layers (Figure 5, bottom).

Optical coherence tomography of 16 lesions from 3 to 7 seconds through 1 minute after laser delivery, and of 14 lesions through 15 minutes after laser delivery, showed a similar pattern of lesion development (Figure 6). The earliest change, first observed between 3 and 22 seconds in 14 of 16 lesions (88%), was a central zone of high reflectivity at the level of the photoreceptors, with a perimeter of low reflectivity at the level of the retinal pigment epithelium and inner choroid (Figure 6, top right). The horizontal size of the lesion did not change from that seen initially. The high reflectivity quickly increased in vertical size within the first 25 seconds, extending from the outer nuclear layer through the nerve fiber layer in 14 of 17 lesions (82%) (Figure 6, top right and bottom left and right). All the lesions demon-

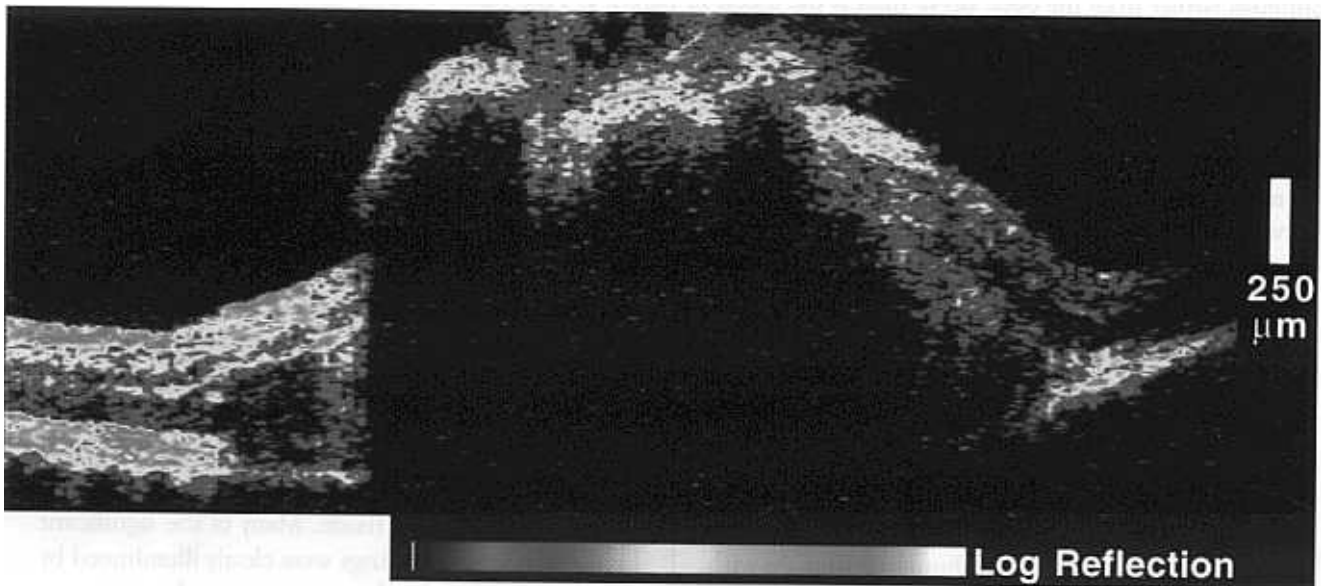


Figure 5. (Top) Light micrographs of 1-hour-old, 500-mW, 200-msec argon laser retinal lesion demonstrates a large subretinal, intraretinal, and vitreous hemorrhage. Retinal layers are grossly displaced by the blood. (Bottom) Optical coherence tomography of the hemorrhagic lesion 3 minutes 40 seconds after argon laser delivery, at a site corresponding to the section at top, demonstrates a bulging area of intense high reflectivity that corresponds to the mass of preretinal blood. There was an intensely low reflectivity "shadow" behind this high reflectivity site, with no images of the typical optical coherence tomography retinal layers.

strated this change within 3 minutes. Although 1-hour lesions demonstrated mild elevation of the inner retinal surface with optical coherence tomography, there was no retinal distortion, separation, or folding, as seen in the light micrographs (Figure 4, left).

DISCUSSION

CORRELATING THE HISTOLOGY OF NORMAL TISSUE AND argon laser lesions in the *M mulatta* retina, we demonstrated the alignment of distinctive retinal and

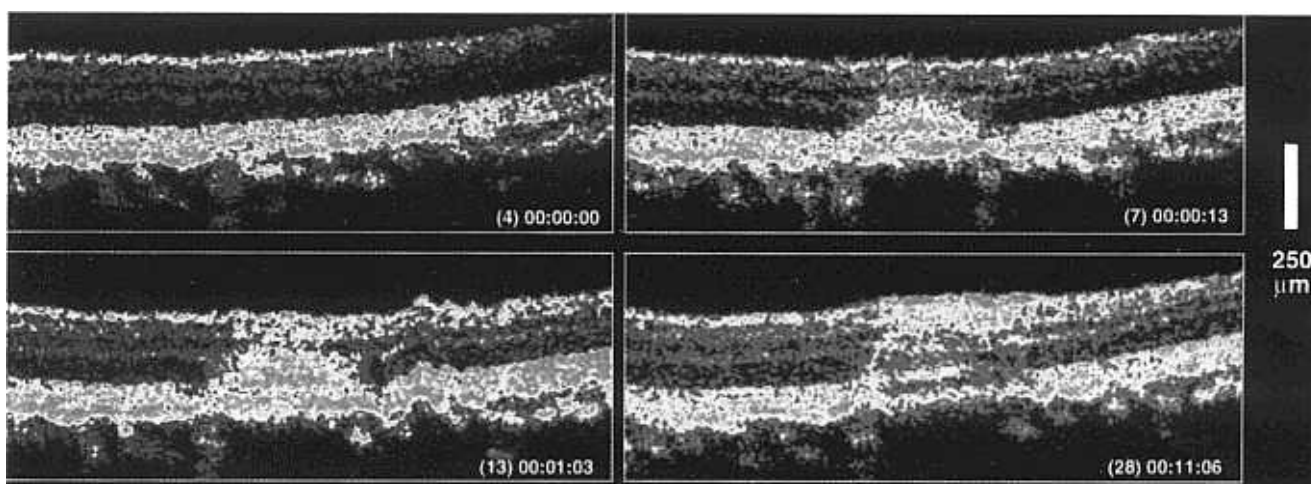


Figure 6. (Top left) Optical coherence tomography of the macular site immediately before argon laser treatment. The retinal layers (high reflectivity corresponding to nerve fiber and plexiform layers, low reflectivity corresponding to nuclear and photoreceptor layers) are typical of the primate macula. The nasal retina is to the left side of the image, although farther from the optic nerve than is the lesion in Figure 1. (Top right) Optical coherence tomography of the 380-mW argon laser retinal lesion at 13 seconds demonstrates a central zone of high reflectivity at the level of the photoreceptors, with a perimeter of low reflectivity at the level of the retinal pigment epithelium and inner choroid. (Bottom, left and right) These optical coherence tomography images demonstrate no change in the horizontal size of the lesion compared with that seen initially at top right. The high reflectivity quickly increased in vertical size within the first 25 seconds (top right and bottom left), extending from the outer nuclear layer through the nerve fiber layer within 11 minutes (bottom right). A border of low reflectivity extends into the choroidal layer beneath the central lesion at 11 minutes.

choroidal elements to particular zones of high reflectivity and low reflectivity identified on optical coherence tomography. This allowed us to analyze changes in optical coherence tomography images acquired over time to map the development of retinal laser lesions.

The morphologic characteristics of the primate retina are similar to those of the human retina. As with all dehydrated histopathologic sections, size is affected by tissue dehydration, and by the embedded tissue stretching when strips are sectioned. Analyzing normal retinal tissue, we consistently found a 5% to 12% increase in size of the final light microscopic image relative to optical coherence tomography image size (Toth CA, Narayan DG, Boppart SA, et al, unpublished data correlating optical coherence tomography and histopathology of normal primate retina, 1996). The thermally mummified argon laser lesions may respond differently to fixation because of changes in penetration of fixative into the lesion. Several of our laser lesions demonstrated clefting and thickening when the sections of fixed tissue were examined using light microscopy. Optical coherence tomography verified some

thickening of retinal laser lesions in vivo and demonstrated in vivo clefting of the nerve fiber layer in one lesion. This study demonstrates that optical coherence tomography can assess laser tissue effects at a level similar to but with less resolution than light microscopy but, most importantly, without the artifacts intrinsic to fixation of the tissue. Many of the significant light microscopic findings were clearly illuminated by the in vivo optical coherence tomography.

Because optical coherence tomography reflective responses and comparable light microscopic images used very different approaches to view cellular elements, the two did not directly compare. Light microscopy, with the variable staining of fixed tissue, in this case by methylene blue dye, can display subcellular microscopic structure. The optical coherence tomography imaging system, on the other hand, does not rely on the same methods of tissue differentiation that histopathology does. Optical coherence tomography, analogous to ultrasound with its pathway of incoming and outgoing signal from a tested tissue, can display focal variations in interferometry from the tissue at a resolution of 10 μm . Optical

coherence tomography assesses relative sites of high and low reflectivity of tissue as measured by signal returned to the instrument. Laser energy may be removed by absorption in the tissue layer under analysis, lateral scattering that is not returned to the probe, and extensive absorption or scatter in media between the optical coherence tomography probe and the site of interest, preventing optical coherence tomography imaging of this site. Thus, in contrast to cross-section histopathology, with optical coherence tomography we saw shadowing from highly reflective material, such as vitreous hemorrhage (Figure 5, bottom) and retinal pigment epithelium, with loss of an image in deeper layers, such as the retina beneath the blood and the choroid beneath the retinal pigment epithelium. Because of the dense pigmentation of the retinal pigment epithelium and choroid in *M. mulatta*, the loss of optical coherence tomography image in the choroid in the normal retina in our study (Figure 6, top left) may have occurred at a shallower penetration compared with optical coherence tomography images of some patients.¹²⁻¹⁴

A site of morphologic abnormality evidenced on light microscopy did not necessarily demonstrate any abnormality when assessed by optical coherence tomography. This was seen at several sites of milder inner retinal damage that did not appear as a significant aberration from normal on optical coherence tomography. The reverse was also demonstrated: there were focal sites of intense high reflectivity corresponding to the photoreceptors damaged centrally in the laser lesion when viewed by optical coherence tomography, yet light microscopy demonstrated only mild morphologic changes in the damaged photoreceptors at 1 day. Perhaps the optical coherence tomography identified a change in the tissue reflectivity that cannot be measured by light microscopy. This study only begins to identify the tissue components affecting the reflectivity response. In future applications, analysis of the output signal from the tissue in response to varying optical coherence tomography laser energy input may allow us to identify some of the factors, such as absorption, refractive index, and scattering, that determine the optical coherence tomography image.

Delineating early morphologic changes at a laser lesion site by optical coherence tomography sampling from the moment of impact throughout the healing

phase provided us with new data about the earliest tissue response to laser treatment. Our analysis demonstrated clearly that some retinal thickening does occur by 1 hour over retinal laser sites at the fluences delivered and that later inner retinal layer splitting also occurs in vivo. We also demonstrated that the earliest retinal effects from argon laser can be seen across the entire breadth of the lesion within seconds after laser delivery, whereas the inner retinal responses, at least as measured by changes in relative reflectivity, are delayed by additional seconds to minutes. Vacuoles of fluid surrounding the laser lesion, seen as a margin of relative low reflectivity around the margins of the highly reflective central lesion, were minimal during the first minutes after laser delivery and increased at 1 and 2 days after laser delivery. The 8-day correlation of the evolution of retinal lesions further demonstrated the association between focal areas of high reflectivity and the presence of retinal pigment epithelium cells that had migrated within the retina. Applying additional image analysis techniques to the patterns of evolving changes in reflectivity at specific retinal sites may allow us to use these patterns as the hallmark of a specific pathologic process, such as increasing edema at the margin of an argon laser lesion.

This nonincisional, noncontact method of evaluation of retinal disease, injury, or response to therapy may be applied in future animal studies of the retina. With sequential imaging of retinal lesions with optical coherence tomography, rather than excision of lesions and euthanasia of study animals at numerous time points to obtain the same sequential data, smaller numbers of animals may be required for research.

This study provides clinicians and researchers with a clinicopathologic correlation of optical coherence tomography images with microscopic pathology of laser lesions, which improves our general understanding of the interpretation of optical coherence tomography images of patients with retinal disease. Thus far, researchers have inferred, from their knowledge of classic histopathology, the possible pathologic processes that have resulted in the optical coherence tomography images.¹¹⁻¹⁷ Our clinicopathologic correlation in the primate demonstrated the association between specific sites of optical coherence tomography-imaged high reflectivity and low reflectivity

and corresponding microscopic pathology, thus improving our clinical acumen in applying this technology.

Our method of rapid-sequence optical coherence tomography, although limited by resolution, provided a sequential cross-sectional image of laser lesion development that also improved our understanding of the evolving tissue response to thermal laser injury. In the earliest time period, there was a lack of lateral spread of the retinal lesion by optical coherence tomography despite significant vertical evolution of the full-thickness lesions. Over a longer time frame, a variety of healing responses to the laser injury, from vacuole formation to cellular infiltration and tissue contraction, was sequentially mapped. Thus we could view the earliest tissue response to a laser dose continuously at that site from the first seconds onward, and we could monitor the timing and extent of the healing response to the initial insult. This demonstrates the potential future uses of optical coherence tomography in ophthalmic research and clinical care to follow acute and long-term macular response to an injury, a disease process, or an ocular therapy. Building on our use of this system to obtain novel sequential information about immediate retinal laser effects, surgeons may eventually use optical coherence tomography data to identify an endpoint or provide direct feedback during laser treatment of macular disease.

ACKNOWLEDGMENTS

We would like to thank Katrina Winter and Ewa Worniallo for their support of the histopathology effort and preparation of the manuscript.

REFERENCES

1. Apple DJ, Goldberg MF, Wyhinny G. Histopathology and ultrastructure of the argon laser lesion in human retinal and choroidal vasculatures. *Am J Ophthalmol* 1973;75:595-609.
2. Borges JM, Charles HC, Lee CM, et al. A clinicopathologic study of dye laser photocoagulation on primate retina. *Retina* 1987;7:46-57.
3. Borland RG, Brennan DH, Marshall J, Viveash JP. The role of fluorescein angiography in the detection of laser-induced damage to the retina: a threshold study for Q-switched, neodymium and ruby lasers. *Exp Eye Res* 1978;27:471-493.
4. Brancato R, Pratesi R, Leoni G, Trabucchi G, Vanni U. Histopathology of diode and argon laser lesions in rabbit retina: a comparative study. *Invest Ophthalmol Vis Sci* 1989;30:1504-1510.
5. Lorenz B. Morphologic changes of chorioretinal argon laser burns during the first hour postexposure. *Lasers Life Sci* 1988;2:207-226.
6. Powell JO, Bresnick GH, Yanoff M, Frisch GD, Chester JE. Ocular effects of argon laser radiation, II: histopathology of chorioretinal lesions. *Am J Ophthalmol* 1971;71:1267-1276.
7. Rosan RC, Flocks M, Vassiliadis A, Rose HW, Peabody RR, Hammond A. Pathology of monkey retina following irradiation with an argon laser. *Arch Ophthalmol* 1969;81:84-88.
8. Smiddy WE, Patz A, Quigley HA, Dunkelberger GR. Histopathology of the effects of tuneable dye laser on monkey retina. *Ophthalmology* 1988;95:956-963.
9. Thomas EL, Apple DJ, Swartz M, Kavka-Van Norman D. Histopathology and ultrastructure of krypton and argon laser lesions in a human retina choroid. *Retina* 1984;4:22-39.
10. Wallow IH, Lund OE, Gabel VP, Birngruber R, Hillenkamp F. A comparison of retinal argon laser lesions in man and in cynomolgus monkey. *Albrecht Von Graefes Arch Klin Exp Ophthalmol* 1974;189:159-164.
11. Hee MR, Puliafito CA, Wong C, et al. Optical coherence tomography of macular holes. *Ophthalmology* 1995;102:748-756.
12. Hee MR, Izatt JA, Swanson EA, et al. Optical coherence tomography of the human retina. *Arch Ophthalmol* 1995;113:325-332.
13. Hee MR, Puliafito CA, Wong C, et al. Optical coherence tomography of central serous chorioretinopathy. *Am J Ophthalmol* 1995;120:65-74.
14. Huang D, Swanson EA, Lin CP, et al. Optical coherence tomography. *Science* 1991;254:1178-1181.
15. Izatt JA, Hee MR, Swanson EA, et al. Micrometer-scale resolution imaging of the anterior eye in vivo with optical coherence tomography. *Arch Ophthalmol* 1994;112:1584-1589.
16. Puliafito CA, Hee MR, Lin CP, et al. Imaging of macular diseases with optical coherence tomography. *Ophthalmology* 1995;102:217-229.
17. Schuman JS, Hee MR, Puliafito CA, et al. Quantification of nerve fiber layer thickness in normal and glaucomatous eyes using optical coherence tomography. *Arch Ophthalmol* 1995;113:586-596.

Authors Interactive™

Comments and questions of 100 words or less regarding this article may be addressed to authors via THE JOURNAL'S Web Site on the Internet. Selected questions and comments along with the authors' statements and responses will be posted on the Authors Interactive™ Bulletin Board, a feature of THE JOURNAL'S home page. Readers may access THE JOURNAL'S home page and the Authors Interactive™ Bulletin Board at <http://www.ajo.com/>